Dalton Transactions

RSC Publishing

PAPER

View Article Online
View Journal | View Issue

Cite this: *Dalton Trans.*, 2013, **42**, 7386

Computational study of the hydrodefluorination of fluoroarenes at [Ru(NHC)$(PR_3)_2(CO)(H)_2$]: predicted scope and regioselectivities†

Stuart A. Macgregor,*[a] David McKay,[a] Julien A. Panetier‡[a] and Michael K. Whittlesey*[b]

Density functional theory calculations have been employed to investigate the scope and selectivity of the hydrodefluorination (HDF) of fluoroarenes, $C_6F_{6-n}H_n$ (n = 0–5), at catalysts of the type [Ru(NHC)-$(PR_3)_2(CO)(H)_2$]. Based on our previous study (*Angew. Chem., Int. Ed.*, 2011, **50**, 2783) two mechanisms featuring the nucleophilic attack of a hydride ligand at a fluoroarene substrate were considered: (i) a concerted process with Ru–H/C–F exchange occurring in one step; and (ii) a stepwise pathway in which the rate-determining transition state involves formation of HF and a Ru-σ-fluoroaryl complex. The nature of the metal coordination environment and, in particular, the NHC ligand was found to play an important role in both promoting the HDF reaction and determining the regioselectivity of this process. Thus for the reaction of C_6F_5H, the full experimental system (NHC = IMes, R = Ph) promotes HDF through (i) more facile initial PR_3/fluoroarene substitution and (ii) the ability of the NHC *N*-aryl substituents to stabilise the key C–F bond breaking transition state through F···HC interactions. This latter effect is maximised along the lower energy stepwise pathway when an *ortho*-H substituent is present and this accounts for the *ortho*-selectivity seen in the reaction of C_6F_5H to give 1,2,3,4-$C_6F_4H_2$. Computed C–F bond dissociation energies (BDEs) for $C_6F_{6-n}H_n$ substrates show a general increase with larger n and are most sensitive to the number of *ortho*-F substituents present. However, HDF is always computed to remain significantly exothermic when a silane such as Me_3SiH is included as terminal reductant. Computed barriers to HDF also generally increase with greater n, and for the concerted pathway a good correlation between C–F BDE and barrier height is seen. The two mechanisms were found to have complementary regioselectivities. For the concerted pathway the reaction is directed to sites with two *ortho*-F substituents, as these have the weakest C–F bonds. In contrast, reaction along the stepwise pathway is directed to sites with only one *ortho*-F substituent, due to difficulties in accommodating *ortho*-F substituents in the C–F bond cleavage transition state. Calculations predict that 1,2,3,5-$C_6F_4H_2$ and 1,2,3,4-$C_6F_4H_2$ are viable candidates for HDF at [Ru(IMes)$(PPh_3)_2(CO)(H)_2$] and that this would proceed selectively to give 1,2,4-$C_6F_3H_3$ and 1,2,3-$C_6F_3H_3$, respectively.

Received 10th December 2012,
Accepted 18th January 2013

DOI: 10.1039/c3dt32962c

www.rsc.org/dalton

Introduction

Substituted aryl fluorides are a key component of many pharmaceuticals and agrochemicals[1] and will be a crucial factor in the continuing search for more effective treatments and products. Current approaches to the synthesis of aryl fluorides commonly employ traditional organic chemistry based on nucleophilic aromatic substitution.[2] However, this approach can have drawbacks, including (i) the need for harsh reaction conditions (with implications for functional group tolerance) and (ii) limited selectivity. New methods enabling the more efficient synthesis of selectively-substituted aryl fluorides are therefore highly desirable.

Transition metal catalysis offers one attractive way to address this problem and three general strategies to implement this approach have been explored. The first (eqn (1)) resembles a cross-coupling reaction in which an aryl halide or triflate is activated at a low-valent metal centre, with X^-/F^- exchange and reductive elimination then leading to the

[a]*Institute of Chemical Sciences, School of Engineering and Physical Sciences, Heriot-Watt University, Edinburgh, EH14 4AS, UK*
[b]*Department of Chemistry, University of Bath, Claverton Down, Bath BA2 7AY, UK. E-mail: s.a.macgregor@hw.ac.uk, m.k.whittlesey@bath.ac.uk*

†Electronic supplementary information (ESI) available: Computed geometries and energies of all species; plots of barriers heights against $\Delta D(C–H)_{rel}$ and associated multiple regression data. See DOI: 10.1039/c3dt32962c

‡Present Address: Department of Chemistry, University of California, Berkeley, CA 94720, USA.

desired aryl fluoride. While the first two steps of this process have ample precedent, the reductive elimination is challenging,[3] although progress has been made with Pd catalysts featuring sterically demanding biphenyl-based phosphine ligands.[4] In the second approach (eqn (2)) an aryl boronate supplies the aryl group and C–F bond formation occurs after oxidation with electrophilic fluorine sources, possibly exploiting a Pd(II)/Pd(IV) cycle.[2b,5] The final approach (eqn (3)) targets nucleophilic C–F functionalisation *via* the selective defluorination of one (or more) C–F bonds in cheap and widely available perfluorinated feedstocks. We focus on this strategy here and specifically fluoroarene hydrodefluorination (HDF; Nuc = H), the simplest example of nucleophilic C–F functionalisation in which a C–F bond is replaced by a C–H bond.

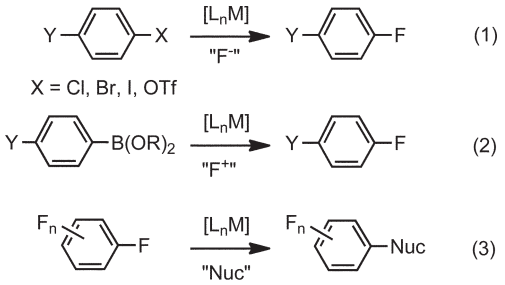

Examples of the stoichiometric HDF of fluoroarenes[6] are known for both early and late transition metals[7] and in many cases involve the reaction of a transition metal hydride to give the corresponding transition metal fluoride and the HDF product. This apparently simple net F/H exchange, however, masks a plethora of mechanistic possibilities. With $[(\eta\text{-}C_5R_5)_2Zr(H)_2]$ both a σ-bond metathesis mechanism (R = H)[8] and the formation of a Meisenheimer intermediate (R = Me)[9] have been postulated. Mechanisms based on single electron transfer processes have also been proposed, both at early[10] and with more electron-rich late transition metals such as *cis*-$[Ru(Me_2PCH_2CH_2PMe_2)_2(H)_2]$[11] or *trans*-$[Pt(PCy_3)_2(H)_2]$.[12] A further variation was seen for $[(\eta\text{-}C_5Me_5)Rh(PMe_3)(H)_2]$ which, after initial deprotonation to give $[(\eta\text{-}C_5Me_5)Rh(PMe_3)(H)]^-$, reacts as a nucleophile at C_6F_6 to give $[(\eta\text{-}C_5Me_5)Rh(PMe_3)(H)(C_6F_5)]$.[13] HDF has also been observed for a lanthanide complex, $[(\eta\text{-}C_5H_2{}^tBu_3)_2Ce(H)]$. In this case density functional theory (DFT) calculations on a $[(\eta\text{-}C_5H_5)_2La(H)]$ model system suggest a novel 'harpoon' mechanism in which a M···FC interaction directs C–F activation to an *ortho*-position, giving $[(\eta\text{-}C_5H_5)_2La(C_6F_5)]$ and HF. Protonolysis then gives the $[(\eta\text{-}C_5H_5)_2La(F)]$ and C_6F_5H products.[14]

In order to develop catalytic HDF the use of a stoichiometric terminal reductant, such as H_2, silanes or aluminium hydrides, is required in order to complete the cycle. These not only remove the fluoride produced in HDF and regenerate the active transition metal hydride species, but also provide a thermodynamic driving force through the formation of strong element–F bonds. The first example of catalytic fluoroarene HDF was reported by Aizenberg and Milstein and involved a $[Rh(PMe_3)_3(SiR_3)]$ species (R_3 = Ph_3, Me_2Ph) and silane reductants;[15] this work was subsequently extended to $[Rh(PMe_3)_3X]$ (X = H, C_6F_5) catalysts with H_2/NEt_3 as reductant.[16] Holland has described the use of [(diketiminato)Fe(F)] catalysts[17] while more recently catalytic HDF of fluoroarenes has been seen at $\{NiL_2\}$ (L = phosphine,[18] or *N*-heterocyclic carbene, NHC[19]) and $\{AuL\}^+$ (L = phosphine, NHC)[20] fragments. These processes all use silanes as the terminal reductant and the Ni and Au systems are thought to proceed *via* initial oxidative addition of a C–F bond. An example of catalytic fluoroarene HDF at $[(\eta\text{-}C_5H_5)_2Zr(Cl)_2]$ using an aluminium hydride terminal reductant has recently been reported.[21]

The above examples refer to HDF of the parent C_6F_6 substrate and in most cases the HDF reaction can be extended to C_6F_5H. Regioselectivity now becomes an issue and most commonly the formation of 1,2,4,5-$C_6F_4H_2$ is observed, arising from HDF at the *para*-position. One example of *ortho*-selectivity was seen in the HDF of C_6F_5H at $[(\eta\text{-}C_5H_2{}^tBu_3)_2Ce(H)]$, and this was rationalised by the 'harpoon' mechanism that directs the site of C–F activation.[14] Extension of HDF beyond C_6F_5H to lower fluorinated species is rare. Johnson has reported the HDF of 1,2,4,5-$C_6F_4H_2$ to give 1,2,4-$C_6F_3H_3$,[18a] while 1,4-$C_6F_2H_4$ is produced upon prolonged heating of C_6F_6 in benzene in the presence of $[Ni_2(IPr)_4(COD)]$[22] and Ph_3SiH.[19] In general, all these systems exhibit low catalytic activities with modest turnover numbers (TON) and frequencies (TOF), even for the most active C_6F_6 substrate.

Recently one of us has reported the catalytic HDF of C_6F_6, C_6F_5H and C_5F_5N using Ru catalysts of the type $[Ru(NHC)(PPh_3)_2(CO)(H)_2]$ (**1**, where NHC = *N*-aryl substituted *N*-heterocyclic carbenes, IMes, SIMes, IPr and SIPr,[22] see Scheme 1).[23] Kinetic studies suggest that catalysis proceeds *via* initial phosphine dissociation to give a 16e intermediate, **2**. HDF then gives the isolable hydride fluoride $[Ru(NHC)(PPh_3)_2(CO)(H)(F)]$, **3**, and silane reduction completes the catalytic cycle. With NHC = SIPr and C_6F_6 TONs of up to 200 (TOF = 0.86 h^{-1}) could be achieved, making this one of the more active HDF catalysts to date. Intriguingly, with C_6F_5H HDF also proceeds with an unexpected *ortho*-selectivity to give 1,2,3,4-$C_6F_4H_2$.

In order to account for these observations we undertook a subsequent DFT study that revealed the HDF reaction to proceed *via* a novel mechanism in which a metal-bound hydride ligand acts as the nucleophile.[24] Calculations on the full $[Ru(IMes)(PPh_3)_2(CO)(H)_2]$ system characterised two pathways, both stemming from the 16e intermediate **2** (Scheme 2): (i) a concerted process *via* **TS(2–3)**, where hydride transfer from Ru displaces fluoride which then migrates back to the metal centre to form 1,2,3,4-$C_6F_4H_2$ and **3** directly; (ii) a stepwise process where the arene initially binds in an η^2-mode (**4**), and then hydride attacks to give a metal-stabilised Meisenheimer intermediate **5** which then goes on to form a σ-aryl species, **6**, with a closely associated molecule of HF. Protonolysis with F transfer to the metal then yields 1,2,3,4-$C_6F_4H_2$ and **3**. This stepwise process is the lower energy route and also accounts for the observed *ortho*-selectivity of this system, the computed activation barrier for the formation of 1,2,3,4-$C_6F_4H_2$ being significantly lower than those for the formation of 1,2,3,5-$C_6F_4H_2$ or 1,2,4,5-$C_6F_4H_2$. The calculations also

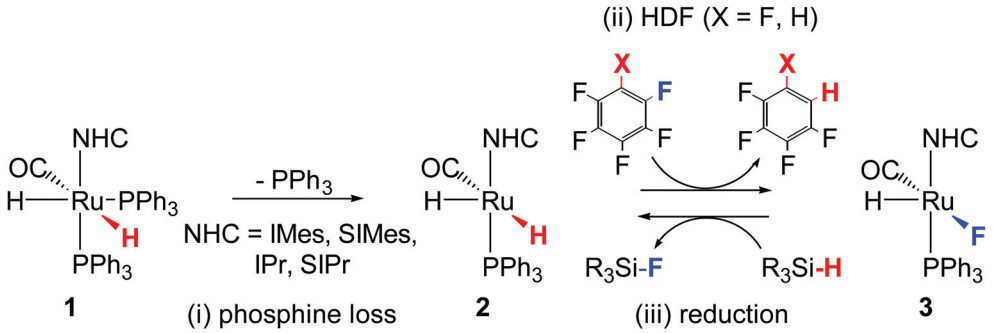

Scheme 1

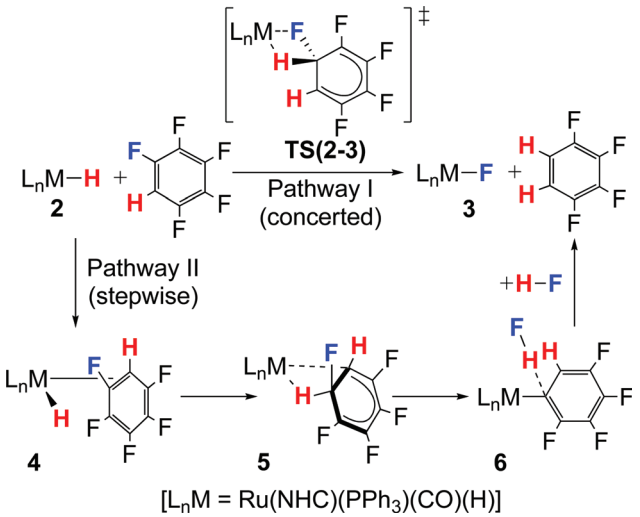

Scheme 2

showed that C–H activation of C_6F_5H, although kinetically accessible, would be reversible, meaning that our system can target C–F activation in the presence of C–H bonds. In addition, an alternative mechanism based on a tetrafluorobenzyne intermediate was ruled out.

In this paper we use density functional theory calculations to explore the origins of the unusual *ortho*-selectivity seen in the HDF reaction of pentafluorobenzene at **1**. Our calculations show that *N*-aryl substituted NHC ligands create a specific environment which favours C–F bond activation, particularly when this occurs *ortho* to a C–H bond. In addition, we provide a general analysis of the HDF reactivity of fluoroarenes, $C_6F_{6-n}H_n$ (n = 0–5), in terms of the computed C–F bond dissociation energies of these species. This is used as the basis to explore the extension of the HDF reaction to lower fluorinated substrates and to predict the regioselectivities associated with these reactions.

Computational details

DFT calculations were run with Gaussian 03 (Revision C.02)[25] and results for the BP86 functional are reported.[26] Ru, P and Si centres were described with the Stuttgart RECPs and associated basis sets,[27] with added d-orbital polarisation on P (ζ = 0.387) and Si (ζ = 0.284).[28] 6-31G** basis sets were used for all other atoms.[29] Test calculations employing a range of functionals and more extended basis sets were also performed and gave similar trends (see Table S1 in the ESI†). All stationary points were fully characterized *via* analytical frequency calculations as either minima (all positive eigenvalues) or transition states (one negative eigenvalue) and IRC calculations and subsequent geometry optimizations were used to confirm the minima linked by each transition state. All energies are corrected for zero-point energy and, in addition, Model 1 includes a solvent correction computed *via* the PCM approach (THF, ε = 7.43).[30] Note that in our initial communication[24] we reported solvent-corrected SCF energies; the reported energies therefore differ slightly between the two studies, although the computed trends are unaffected.

Results and discussion

Mechanism of HDF

We first summarise the key results from our previous study on the mechanism of HDF of C_6F_5H with [Ru(IMes)$(PPh_3)_2$(CO)$(H)_2$], **1**, to give 1,2,3,4-$C_6F_4H_2$. The computed reaction profile is shown in Fig. 1 and we consider first the data in bold for Model 1, equating to solvent-corrected enthalpies for the full experimental system. The most accessible stepwise pathway starts from 16e [Ru(IMes)(PPh_3)(CO)$(H)_2$], **2** (E_{THF} = +23.1 kJ mol^{-1}), formed from **1** *via* initial PPh_3 dissociation, which can then bind C_6F_5H to give π-arene complex, $\mathbf{4}_{ortho}$ (E_{THF} = +36.2 kJ mol^{-1}). Intramolecular nucleophilic attack of the *cis* hydride ligand at the bound arene results in the formation of species $\mathbf{5}_{ortho}$ (E_{THF} = +66.6 kJ mol^{-1}), in which the $\{C_6F_5H_2\}$ moiety resembles a Meisenheimer intermediate that is stabilised by interaction with the Ru centre. C–F bond cleavage then proceeds *via* $\mathbf{TS(5–6)}_{ortho}$ (E_{THF} = +83.6 kJ mol^{-1}) which features a lengthening of the C1···F1 distance to 1.95 Å (see also Fig. 2(a)) and a significant computed (NBO) negative charge of −0.55 associated with F1. Characterisation of $\mathbf{TS(5–6)}_{ortho}$ shows that this highly fluoridic centre is able to deprotonate the incipient $\{C_6F_4H_2\}$ moiety leading to the

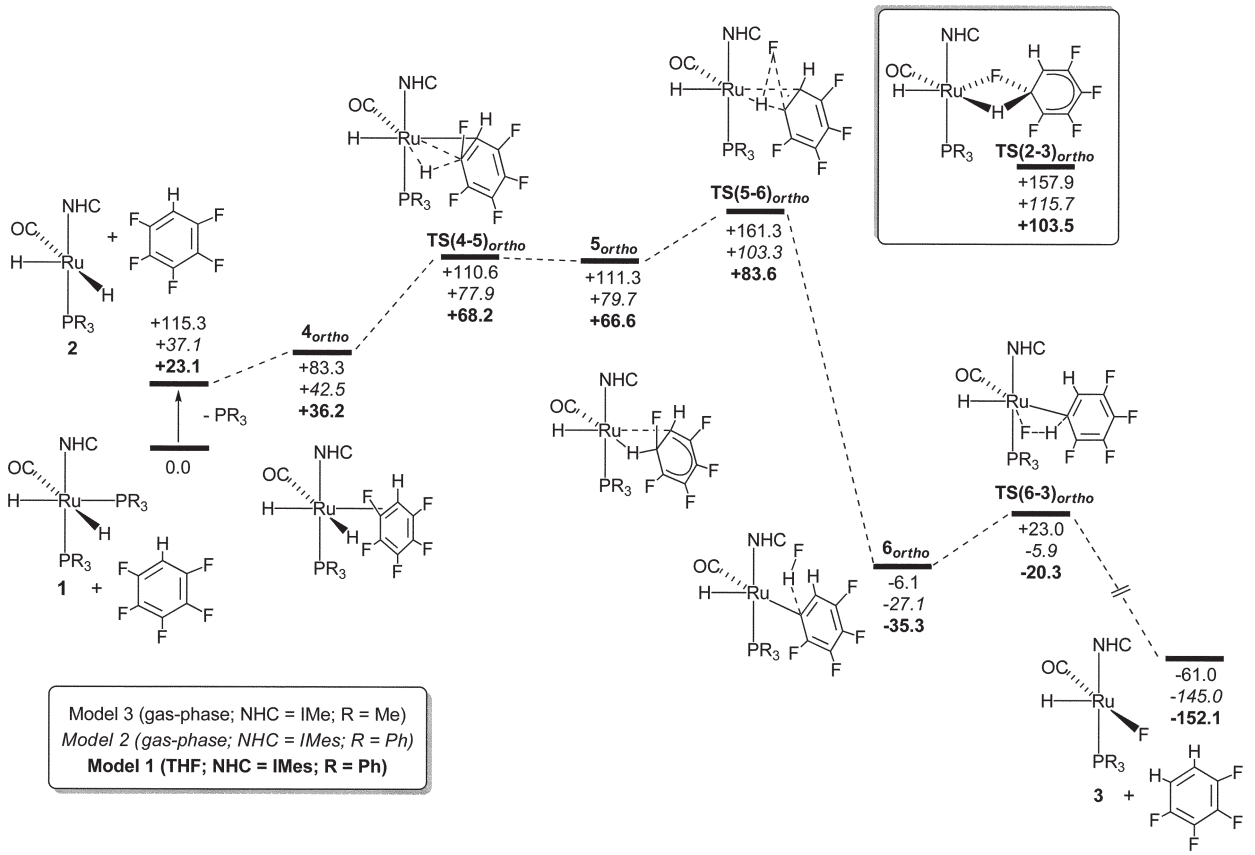

Fig. 1 Computed reaction profiles (kJ mol^{-1}) for HDF at the *ortho*-position of C_6F_5H with different models of $[Ru(NHC)(PR_3)_2(CO)(H)_2]$, **1**.

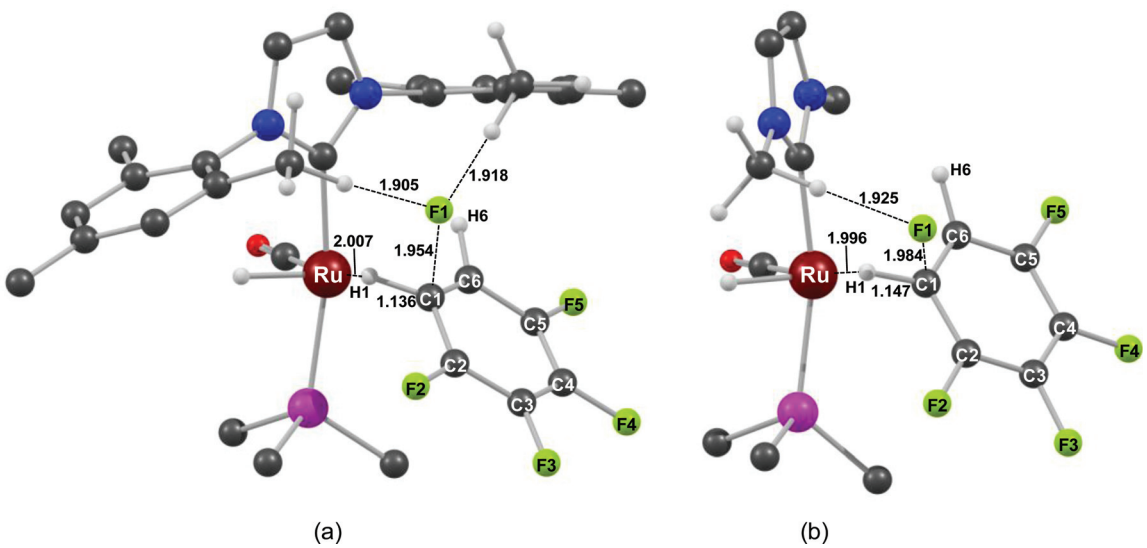

Fig. 2 Computed structures of (a) **TS(5–6)$_{ortho}$** and (b) **TS(5′–6′)$_{ortho}$** with key distances (Å). PR_3 ligands are truncated at the first substituent carbon and NHC hydrogen atoms (with the exception of those Me substituents exhibiting close contacts to F1) are omitted for clarity.

formation of a Ru-σ-aryl complex, $[Ru(IMes)(PPh_3)(CO)(o\text{-}C_6F_4H)(H)]\cdot HF$ (**6$_{ortho}$**, E_{THF} = −35.3 kJ mol^{-1}), featuring a close C1···HF contact. The final step is protonolysis of **6$_{ortho}$**, with HF adding over the Ru–C_6F_4H bond to give $[Ru(IMes)(PPh_3)(CO)(H)(F)]$, **3**, and 1,2,3,4-$C_6F_4H_2$ (E_{THF} = −152.1 kJ mol^{-1}). An alternative concerted pathway was also characterised in which **2** reacts directly with C_6F_5H *via* intermolecular nucleophilic attack of hydride, giving **3** and 1,2,3,4-$C_6F_4H_2$ in one step. In this case the transition state, **TS(2–3)$_{ortho}$** (E_{THF} = +103.5 kJ mol^{-1}), again features a nucleophilic attack of the

hydride ligand, but the different orientation of the arene moiety permits the direct transfer of the displaced fluoride back to the metal centre (see Fig. S1†). The overall barriers for the stepwise and concerted pathways are 83.6 kJ mol^{-1} and 103.5 kJ mol^{-1}, respectively, indicating a kinetic preference for the intramolecular stepwise reaction pathway.[31]

To probe the role of the metal coordination environment and solvent in promoting the HDF reaction we have considered two further computational model systems: Model 2, the full experimental system as before, but with energies computed in the gas-phase (data in italics, Fig. 1); and Model 3, gas-phase computed energies for the smaller model system, [Ru(IMe)-(PMe$_3$)$_2$(CO)(H)$_2$],[22] **1′** (data in plain text, Fig. 1, the prime denoting use of this small model throughout). The relative energy computed for **TS(5–6)$_{ortho}$** increases considerably upon both removal of the solvent correction (E_{gas} = +103.3 kJ mol^{-1}) and use of the small model system (E'_{gas} = +161.3 kJ mol^{-1}). This difference between Models 2 and 3 partly reflects the greater ease of PR$_3$/C$_6$F$_5$H substitution in the larger Model 2. Thus the formation of intermediate **4$_{ortho}$** (+PR$_3$) from **1** (+C$_6$F$_5$H) costs 42.5 kJ mol^{-1} with Model 2, but increases to 83.3 kJ mol^{-1} with Model 3, and this presumably arises from the greater steric bulk of PPh$_3$ and IMes compared to PMe$_3$ and IMe. A difference of 32 kJ mol^{-1} persists in the relative energies of intermediate **5$_{ortho}$** with these two models, but for **TS(5–6)$_{ortho}$** the gap increases to 58 kJ mol^{-1}, indicating that an additional effect that must further favour the full experimental system.

As mentioned above, the structure of **TS(5–6)$_{ortho}$** computed with the full experimental system shows an elongation of the C1–F1 bond, with F1 being displaced towards the IMes ligand, approximately parallel to the Ru–C$_{NHC}$ bond. The large negative charge at F1 results in the appearance of two short, stabilising F1···HC contacts of *ca.* 1.91 Å to the *ortho*-Me substituents of the IMes ligand. In contrast, with Model 3 the IMe ligand in **TS(5′–6′)$_{ortho}$** can only accommodate one such stabilising contact to one of the Me substituents (1.93 Å; the shortest distance to the other Me substituent is over 5.5 Å, see Fig. 2(b)). The lower overall barrier computed with Model 2 compared to Model 3 therefore arises from two effects: (i) easier substitution of phosphine; and (ii) the ability of the bulky *N*-aryl substituted NHC ligand to stabilise the key C–F bond breaking transition state through stabilising F···HC contacts. The overall barrier is also sensitive to the inclusion of solvent effects, the computed barrier reducing by a further 20 kJ mol^{-1} in moving from Model 2 to Model 1.

Origins of the *ortho*-selectivity

Table 1 gives activation barriers computed *via* the stepwise pathway for the competing HDF reactions of C$_6$F$_5$H at the *meta*-position (giving 1,2,3,5-C$_6$F$_4$H$_2$) and at the *para*-position (giving 1,2,4,5-C$_6$F$_4$H$_2$) for Models 1, 2 and 3. For Model 1 the higher barriers computed for these processes (95.9 kJ mol^{-1} and 95.5 kJ mol^{-1} respectively) are consistent with preferential reaction at the *ortho*-position to give 1,2,3,4-C$_6$F$_4$H$_2$ as the dominant species formed experimentally.[32] The higher

Table 1 Computed activation barriers (kJ mol^{-1}) for competing HDF reactions of C$_6$F$_5$H at [Ru(NHC)(PR$_3$)$_2$(CO)(H)$_2$] with Models 1, 2 and 3

	ortho	*meta*	*para*
Model 1	83.6	95.9	95.5
Model 2	103.3	132.0	129.5
Model 3	161.3	176.6	169.1

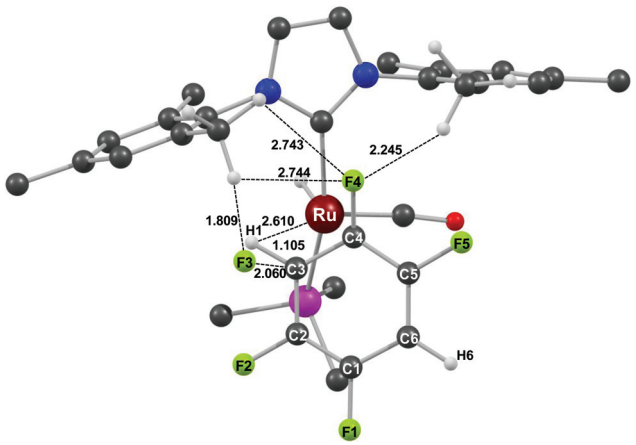

Fig. 3 Computed structure of **TS(5–6)$_{para}$** with key distances (Å). PPh$_3$ ligands are truncated at the first substituent carbon and NHC hydrogen atoms (with the exception of those Me substituents exhibiting close contacts to F3 and F4) are omitted for clarity.

barriers to *meta*- and *para*-C–F activation again reflect the ability of the system to stabilise the fluoridic centre formed during the C–F bond cleavage transition state. Thus in **TS(5–6)$_{para}$** (Fig. 3) the breaking C3–F3 bond is oriented to one side of the NHC ligand, permitting only one short contact of 1.81 Å with an *ortho*-Me hydrogen of the IMes ligand. In this case the central position over the Ru–NHC bond is blocked by the spectator C4–F4 bond. Despite extensive searches we have not been able to locate a transition state in which the C3–F3 bond occupies this position, with all attempts converging on less symmetric structures such as that shown in Fig. 3. The presence of only one F···HC contact is also a feature of **TS(5–6)$_{meta}$**. The implication is that the HDF of fluoroarenes at [Ru(IMes)(PPh$_3$)$_2$(CO)(H)$_2$] will be directed towards centres with at least one *ortho* C–H bond.

It is useful to compare how the different models capture the trends in barriers to HDF. For Model 3 reaction at the *ortho*-position is favoured, although only by about 8 kJ mol^{-1} over the *para*-position. As detailed above, the inclusion of the bulky IMes and PPh$_3$ ligands in Model 2 significantly reduces the barrier to HDF at the *ortho*-position by 58 kJ mol^{-1}. This effect is less important for the *meta*- and *para*-positions, the reduction in barrier being only *ca.* 40 kJ mol^{-1}. This reflects the lack of any extra stabilisation gained in **TS(5–6)$_{para}$** and **TS(5–6)$_{meta}$** in moving from IMe to IMes: in these cases both NHCs can only accommodate one short F···HC contact. The 40 kJ mol^{-1} stabilisation that is computed for **TS(5–6)$_{para}$** and **TS(5–6)$_{meta}$** primarily reflects the easier PR$_3$/C$_6$F$_5$H

substitution step. In contrast, the inclusion of a solvent correction is more stabilising for **TS(5–6)$_{para}$** and **TS(5–6)$_{meta}$**. This arises from the less symmetric geometries of these species which leads to them having larger dipole moments (8.06 D and 8.77 D, respectively, *cf.* 5.26 D for **TS(5–6)$_{ortho}$**). These structures are therefore subject to greater stabilisation by the solvent dielectric and as a result, although Model 1 still favours HDF at the *ortho*-position, the barriers for reaction at the *meta*- and *para*-positions are only *ca.* 12 kJ mol^{-1} higher in energy.

Another factor affecting the energy of these HDF transition states is the orientation of the fluoroarene. The lowest energy form of **TS(5–6)$_{ortho}$** considered so far has the C6–H6 bond oriented toward the IMes ligand (see Fig. 4(a)) and for Model 1 this arrangement is 42 kJ mol^{-1} more stable than the alternative where the C2–F2 is in this position (Fig. 4(b)). With **TS(5–6)$_{meta}$** the effect is much smaller as the C–H bond is more remote from the steric bulk of the ligands; in this case the preferred orientation actually has the C–H bond oriented towards the phosphine, this being 10 kJ mol^{-1} more stable than when it is directed towards the NHC. For **TS(5–6)$_{para}$** only one orientation of the C6–H6 is possible. In the following, for calculations on the full model we will only report the more stable form of these two types of transition states.

In summary, the NHC ligand is a key factor in directing the regioselectivity of HDF of C_6F_5H. The steric bulk of the *N*-aryl NHCs favours a substrate orientation that directs an *ortho*-C–H bond towards the NHC; in addition the ability of the NHC substituents to stabilise the cleaving C–F bond is maximised when C–F activation occurs *ortho* to a C–H bond. While other factors such as solvent polarity promote HDF *meta* or *para* to a C–H bond, overall for C_6F_5H the favoured site is at the *ortho*-position to give 1,2,3,4-$C_6F_4H_2$, as seen experimentally.

HDF of lower fluorinated substrates

(a) Thermodynamics. The intrinsic properties of the full series of $C_6F_{6-n}H_n$ (n = 0–5) substrates have been considered in order to define how the number of fluorine substituents affects the energetics of HDF and also how the pattern of substitution determines regioselectivity. Eqn (4) shows the overall process for catalytic HDF and includes the favourable transformation of a silane to a fluorosilane (here Me_3SiH to Me_3SiF) that is necessary to regenerate catalytically-active [Ru(IMes)-(PPh_3)(CO)$(H)_2$], **2**, from [Ru(IMes)(PPh_3)(CO)(H)(F)], **3**. As the energy of the Me_3SiH to Me_3SiF transformation will be constant, the trends in the thermodynamics of HDF will reflect the strength of the C–F bonds being broken and the C–H bonds being formed.

$$C_6F_{6-n}H_n\ (n = 0\text{–}5) + Me_3Si\text{–}H \rightarrow C_6F_{5-n}H_{1+n} + Me_3Si\text{–}F \quad (4)$$

Previously, Clot, Eisenstein, Perutz and co-workers have investigated trends in C–H bond strengths in fluoroarenes and revealed a strong dependence on the number of *ortho*-F substituents present.[33] They used multiple regression techniques to show that the homolytic bond dissociation energy (BDE) of a C–H bond is increased by an average of 10.4 kJ mol^{-1} upon replacement of an *ortho* hydrogen by fluorine. The effects of H/F replacement at the *meta*- or *para*-positions were much smaller, increasing the C–H BDE by only 0.3 kJ mol^{-1} and 3.4 kJ mol^{-1} respectively. Here, we apply a similar approach to the computed C–F homolytic BDEs for the 20 unique C–F bonds in the $C_6F_{6-n}H_n$ (n = 0–5) series.[34] The results of the multiple regression analysis on the C–F BDEs are shown in Fig. 5(a), in which $\Delta D(\text{C–F})_{\text{rel}}$ is the computed C–F BDE relative to that of the C3–F3 (*i.e. para*-C–F) bond in C_6F_5H. Equivalent C–H bond data are shown in Fig. 5(b), where $\Delta D(\text{C–H})_{\text{rel}}$ is relative to the C–H bond in C_6F_5H (these data differ slightly from those reported with the earlier B3PW91 study[33] as they have been recomputed here with the BP86 functional and include a correction for zero-point energy). In contrast to the C–H bonds, the trend in C–F BDEs shows a general strengthening as the number of fluorine substituents is reduced.[35] As with the C–H BDEs, the C–F BDEs depend most significantly on the number of *ortho*-F substituents, x (x = 0, 1, 2), with F/H replacement causing a increase in C–F BDE by 7.5 ± 0.2 kJ mol^{-1}, while at the *meta*- and *para*-positions the average increases in BDE upon F/H replacement are 2.2 ± 0.2 kJ mol^{-1} and 0.8 ± 0.3 kJ mol^{-1}, respectively. While still dominant, the relative influence of the *ortho*-position is less marked than for the C–H BDEs. As a result the C–F BDE data are more evenly spread and do not show the marked clustering into three distinct groups (depending on the number of *ortho*-Fs present) that was a feature of the data for C–H BDEs.

Both trends in the relative C–F and C–H BDEs indicate that HDF will become progressively harder for substrates with fewer fluorine substituents, as both the C–F bond being broken will tend to be stronger and the new C–H bond being formed will tend to be weaker. This is further illustrated in Fig. 6 which plots the energy required to break the substrate C–F bond against the energy released upon forming the new C–H bond. The most favourable HDF processes are for highly fluorinated species, *e.g.* (i) C_6F_6 (C–F = 531.9 kJ mol^{-1}) to C_6F_5H (C–H = 487.3 kJ mol^{-1}) while HDF of C_6FH_5 (vi) is least favoured (C–F = 552.4 kJ mol^{-1}) to C_6H_6 (C–H = 462.5 kJ mol^{-1}). The total spread of BDEs for the C–F and C–H BDEs is rather similar (22 kJ mol^{-1} and 25 kJ mol^{-1} respectively) and as these trends reinforce each other the total variation in the

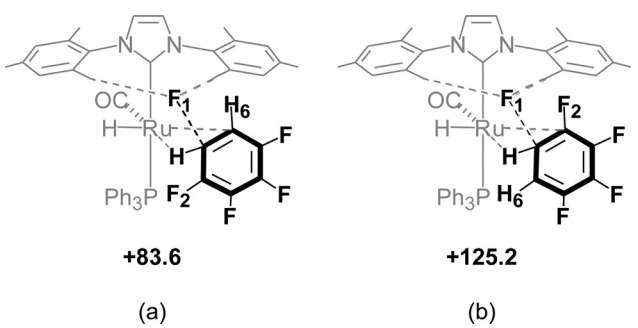

Fig. 4 Alternative orientations of the fluoroarene in **TS(5–6)$_{ortho}$**, with relative energies in kJ mol^{-1} computed with Model 1.

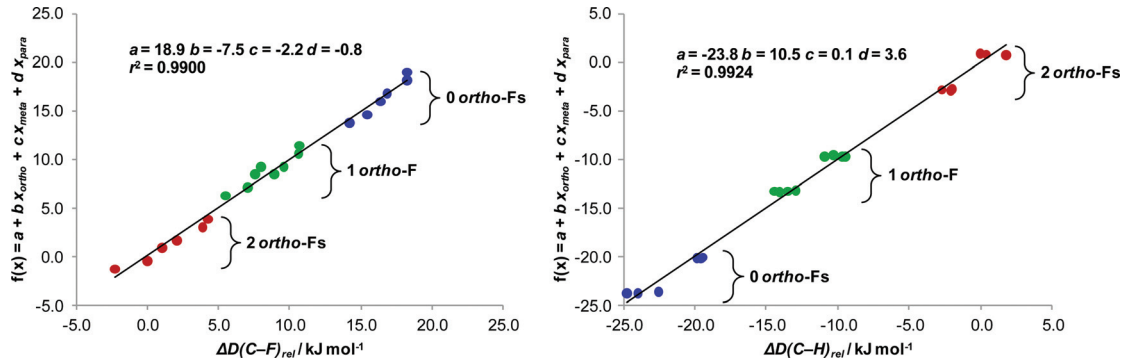

Fig. 5 Plots of (a) $f(x)$ *vs.* $\Delta D(\text{C–F})_{\text{rel}}$ and (b) $f(x)$ *vs.* $\Delta D(\text{C–H})_{\text{rel}}$ for fluoroarenes $C_6F_{6-n}H_n$ (n = 0–5).

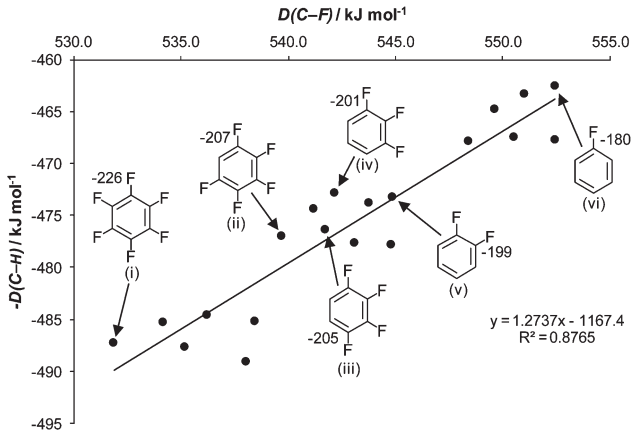

Fig. 6 Plot of energy required for C–F bond cleavage, D(C–F), *vs.* energy released due to C–H bond formation, $-D$(C–H), upon HDF of $C_6F_{6-n}H_n$ species (n = 0–5). The overall energy change for HDF (*cf.* eqn (4)) is highlighted for selected C–F bonds.

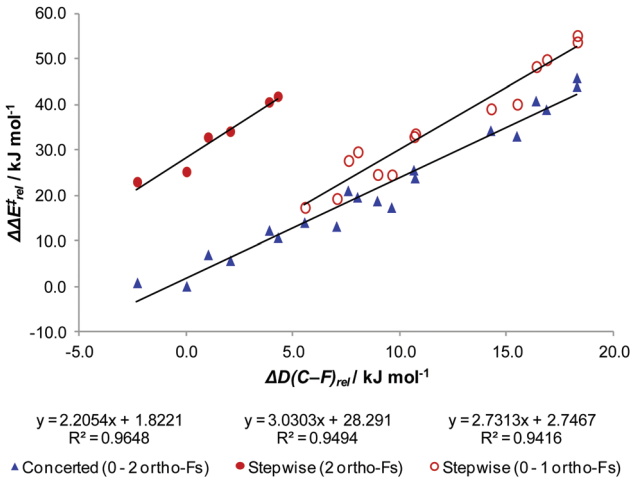

Fig. 7 Plots of $\Delta\Delta E^{\ddagger}_{\text{rel}}$ *vs.* $\Delta D(\text{C–F})_{\text{rel}}$ for $C_6F_{6-n}H_n$ (n = 0–5) computed with $[Ru(IMe)(PMe_3)_2(CO)(H)_2]$ (Model 3, see text for details).

overall computed enthalpy change for HDF is around 47 kJ mol^{-1}. Despite this, HDF is always exothermic as it includes the very favourable formation of Me_3SiF (*cf.* eqn (4)). Selected computed energy changes associated with eqn (4) are highlighted for some substrates in Fig. 6 and range from −226 kJ mol^{-1} for C_6F_6 to −180 kJ mol^{-1} for C_6FH_5.

(b) Kinetics. With C_6F_5H the rate limiting HDF transition states along the stepwise and concerted pathways both feature different degrees of C–F bond elongation (*e.g.* **TS(5–6)$_{ortho}$**: C1···F1 = 1.95 Å; **TS(2–3)$_{ortho}$**: C1···F1 = 1.46 Å). Elongation of the C–H distance is also computed, although this is now more marked along the concerted pathway (**TS(2–3)$_{ortho}$**: C1···H1 = 1.47 Å) rather than the stepwise pathway (**TS(5–6)$_{ortho}$**: C1···H1 = 1.14 Å). To assess how these variations are reflected in the overall barriers to HDF and the regioselectivity of this process, we have located **TS(5–6)** and **TS(2–3)** for the full $C_6F_{6-n}H_n$ (n = 0–5) series. For this we have employed the small Model 3, *i.e.* $[Ru(IMe)(PMe_3)_2(CO)(H)_2]$, which allows us to focus primarily on electronic effects;[36] the full experimental system will be considered for selected substrates in the following section. Fig. 7 plots computed activation barriers, $\Delta\Delta E^{\ddagger}_{\text{rel}}$, against $\Delta D(\text{C–F})_{\text{rel}}$ of the cleaving C–F bond (where $\Delta\Delta E^{\ddagger}_{\text{rel}}$ is relative to the barrier for HDF at the C3–F3 bond of C_6F_5H *via* the concerted mechanism), while computed activation barriers for both mechanisms are reported in Fig. 8.

For the concerted mechanism a good correlation (R^2 = 0.965) between $\Delta\Delta E^{\ddagger}_{\text{rel}}$ and $\Delta D(\text{C–F})_{\text{rel}}$ is seen across the whole range of substrates, with a general increase in barrier as the number of fluorine substituents decreases. In contrast, a plot of $\Delta\Delta E^{\ddagger}_{\text{rel}}$ *vs.* $\Delta D(\text{C–H})_{\text{rel}}$ shows the C–H BDE is less important (R^2 = 0.809, see Fig. S4†). The nature of the *ortho*-substituent is again the most important factor in determining regioselectivity, with HDF *via* the concerted mechanism most likely to occur at sites with two *ortho*-F substituents, as these feature the weakest C–F bonds. Indeed a multiple regression analysis of barrier height against the substituent pattern indicates *ortho*-H/F substitution lowers the barrier by an average of 17 kJ mol^{-1}, *meta*-H/F substitution lowers it by 6 kJ mol^{-1}, but *para*-H/F substitution actually raises the barrier by 2 kJ mol^{-1}. Thus for C_6F_5H, reaction at the (*para*) C3-position is favoured and clear kinetic preferences for reaction at the 2-position are predicted for 1,2,3,4-$C_6F_4H_2$ and 1,2,3-$C_6F_3H_3$ (see plain text data in Fig. 8). For 1,2,3,5-$C_6F_4H_2$ reaction at 2-position is only marginally favoured over the 1-position. This reflects a balance

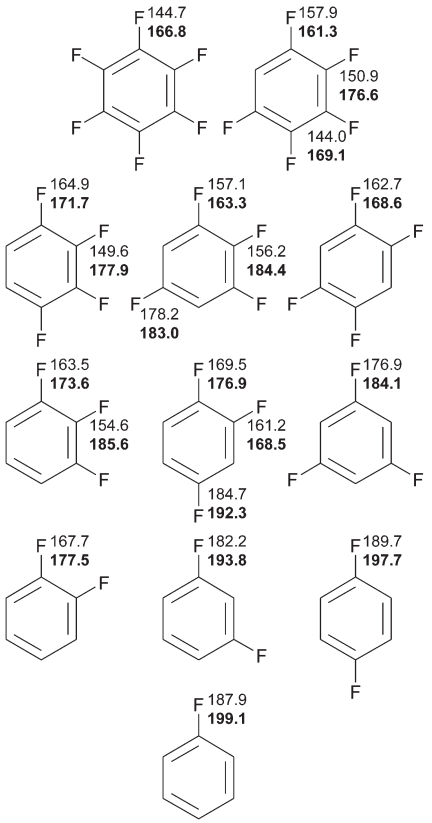

Fig. 8 Computed activation barriers (kJ mol^{-1}) for HDF of $C_6F_{6-n}H_n$ species (n = 0–5) at [Ru(IMe)$(PMe_3)_2$(CO)$(H)_2$] (Model 3). Data in bold are for the stepwise pathway and those in plain text are for the concerted pathway.

of directing effects: at the 2-position the presence of two *ortho*-Fs promotes HDF but this is mitigated by the *para*-F; at the 1-position the combination of one *ortho*-F and two *meta*-Fs (and no *para*-F) results in only a slightly higher barrier. Overall, these predicted selectivities are similar to those observed for the majority of examples of transition metal mediated HDF of fluoroarenes. Indeed we expect our analysis to be quite general and to apply in cases where the C–F BDE is the factor that dominates the reactivity of a fluoroarene.

For the stepwise process the computed activation data fall into two distinct sets, depending on the number of *ortho*-Fs (x = 0, 1 or x = 2). In both cases the trend towards increased activation barriers with lower number of F substituents is again seen, with good correlations between $\Delta\Delta E^{\ddagger}_{rel}$ and $\Delta D(\text{C–F})_{rel}$ (x = 0, 1: R^2 = 0.942; x = 2: R^2 = 0.949). The C–F BDE is again the dominant factor, as there is no correlation with $\Delta D(\text{C–H})_{rel}$ for x = 2 (R^2 = 0.012) or this is weak for x = 0, 1 (R^2 = 0.733, see Fig. S4†). In general with the small Model 3 $\Delta\Delta E^{\ddagger}_{rel}$ is larger for the stepwise rather than the concerted pathway, although for x = 0 or 1 the two pathways do become competitive with the higher fluorinated substrates (*e.g.* the 1-position of C_6F_5H). For x = 2 all transition state structures are destabilized by the need to accommodate an *ortho*-F substituent near to the reacting C–F bond, and this results in a *ca.* 25 kJ mol^{-1} increase in $\Delta\Delta E^{\ddagger}_{rel}$ compared to the equivalent reaction *via* the concerted pathway. The regioselectivity of HDF is therefore completely different to that seen for the concerted pathway as now the presence of two *ortho*-Fs increases barriers and reaction is actually preferred at sites that have one *ortho*-F. Thus, as discussed above, HDF at C_6F_5H *via* the stepwise pathway favours the (*ortho*) C1-position and similarly the 1-position is kinetically preferred for 1,2,3,4-$C_6F_4H_2$, 1,2,3,5-$C_6F_4H_2$ and 1,2,3-$C_6F_3H_3$ (see data in bold text, Fig. 8). 1,2,4-$C_6F_3H_3$ provides an interesting example where the substrate has two distinct C–F bonds, each of which has one *ortho*-F substituent. In this case the regioselectivity is governed by the *meta*-substituents: the F4 substituent (*meta* to C2) weakens the C2–F2 bond and so favours HDF at this position over C1 (which has no *meta*-F substituents).

Predicted scope and regioselectivity of HDF at [Ru(IMes)$(PPh_3)_2$(CO)$(H)_2$], 1

The results on the $C_6F_{6-n}H_n$ series with [Ru(IMe)$(PMe_3)_2$(CO)$(H)_2$] (Model 3) indicate that the kinetic selectivity of HDF will in many cases change depending on the mechanism that is in operation. The calculations indicate the concerted pathway is favoured and so HDF is kinetically most accessible at sites with two *ortho*-F substituents. In contrast, the stepwise pathway favours sites with one *ortho*-F. We have already shown that the barrier to HDF along the stepwise pathway is significantly reduced by use of the bulkier IMes and PPh_3 ligands as in [Ru(IMes)$(PPh_3)_2$(CO)$(H)_2$]. There is therefore the opportunity to achieve different regiochemical outcomes for HDF by varying the nature of the NHC ligand.

To test these ideas we have computed the overall barriers for the HDF reactions of a range of lower fluorinated substrates at [Ru(IMes)$(PPh_3)_2$(CO)$(H)_2$]. The activation barriers computed with Model 1 are given in Fig. 9 and show that in all cases the stepwise pathway provides the lowest energy HDF process.[37] The most reactive C–F bond is the C1–F1 bond of C_6F_5H, the computed barrier of 83.6 kJ mol^{-1} being slightly below that for C_6F_6 (87.8 kJ mol^{-1}). This reflects a preference for an *ortho*-H substituent (maximising the stabilisation of **TS(5–6)** through two F···CH interactions) over an *ortho*-F substituent that will tend to weaken the reacting C–F BDE. As expected, activation barriers tend to increase with lower fluorinated substrates, although with 1,2,3,4-$C_6F_4H_2$ and 1,2,3,5-$C_6F_4H_2$ barriers of 94.5 kJ mol^{-1} and 84.4 kJ mol^{-1} suggest reaction could still be accessible. Significantly these barriers are for reaction adjacent to an *ortho*-H, to give 1,2,3-$C_6F_3H_3$ and 1,2,4-$C_6F_3H_3$, respectively. We therefore predict that both processes could be accessible with [Ru(NHC)$(PPh_3)_2$(CO)$(H)_2$] catalysts and that if they do proceed they will retain the unusual *ortho*-selectivity that was first highlighted in our study of HDF of C_6F_5H. Experimental studies to probe these processes are underway.

Conclusions

Density functional theory calculations have been employed to investigate the scope and selectivity of the hydrodefluorination

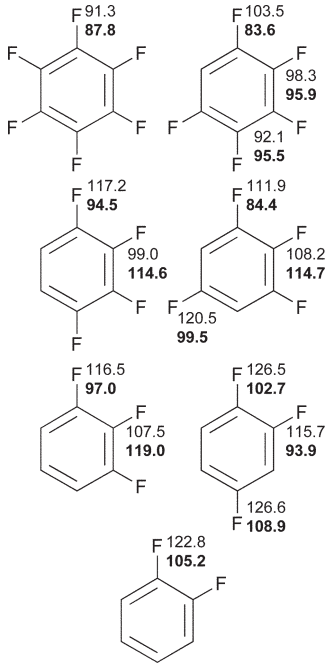

Fig. 9 Activation barriers (kJ mol^{-1}) for HDF of selected $C_6F_{6-n}H_n$ species at [Ru(IMes)$(PPh_3)_2$(CO)$(H)_2$] computed with Model 1. Values in bold are for the stepwise pathway and those in plain text are for the concerted pathway.

(HDF) of fluoroarenes, $C_6F_{6-n}H_n$, (n = 0–5) at catalysts of the type [Ru(NHC)$(PR_3)_2$(CO)$(H)_2$]. The calculations characterise two mechanisms for the HDF process, each based on nucleophilic attack of a hydride ligand at the fluoroarene substrate. The first involves a concerted process with Ru–H/C–F exchange occurring in one step, while the second is a stepwise pathway in which the rate-determining C–F bond cleavage transition state leads to formation of HF and a Ru-σ-fluoroaryl complex. For the reaction of C_6F_5H, comparison of the full experimental system (NHC = IMes, R = Ph) with a small model system (NHC = IMe, R = Me) shows that HDF is promoted experimentally through (i) more facile initial PR_3/fluoroarene substitution and (ii) the ability of the NHC ligand to stabilise the key C–F bond breaking transition state along the stepwise pathway through stabilising F···HC interactions. This latter effect is maximised when the site of HDF has an *ortho*-H substituent and so accounts for the *ortho*-selectivity seen in the reaction of C_6F_5H to give 1,2,3,4-$C_6F_4H_2$.

An analysis of trends in the C–F bond dissociation energies (BDE) in $C_6F_{6-n}H_n$ (n = 0–5) species shows that these generally become stronger with larger n and that the most important factor in determining the BDE is the number of *ortho*-F substituents. The combination of this with the opposite trend in the C–H BDEs means that the thermodynamics of HDF become somewhat less favourable with increased n. However, this process is always significantly exothermic when driven by a silane such as Me_3SiH as terminal reductant. Computed barriers also generally increase with greater n, and for the concerted pathway a good correlation between C–F BDE and barrier height is seen. In this case reaction is directed to sites with two *ortho*-F substituents, as these have the weakest C–F bonds. For the stepwise pathway, the difficulty of accommodating *ortho*-F substituents in the key C–F bond cleavage transition state means that the reaction is directed to sites with only one *ortho*-F substituent. Thus the two mechanisms have complementary regioselectivities. Calculations on the HDF of lower fluorinated substrates (n > 1) at [Ru(IMes)$(PPh_3)_2$(CO)$(H)_2$] predict that 1,2,3,4-$C_6F_4H_2$ and 1,2,3,5-$C_6F_4H_2$ are the most viable targets for this process and that these would both react with *ortho*-selectivity to give 1,2,3-$C_6F_3H_3$ and 1,2,4-$C_6F_3H_3$, respectively.

Acknowledgements

We thank University of Bath and Heriot-Watt University for support, Heriot-Watt University and the EPSRC for provision of a DTA studentship (JAP) and for supporting this work through grant award EP/J010677/1 (DMcK).

References

1 (*a*) J. H. Clark, D. Wails and T. W. Bastock, *Aromatic Fluorination*, CRC Press, Boca Raton, Florida, 1996; (*b*) C. Isanbor and D. O'Hagan, *J. Fluorine Chem.*, 2006, **127**, 303–319; (*c*) A. M. Thayer, *Chem. Eng. News*, 2006, **84**, 15–24; (*d*) W. K. Hagmann, *J. Med. Chem.*, 2008, **51**, 4359–4369; (*e*) S. Purser, P. R. Moore, S. Swallow and V. Gouverneur, *Chem. Soc. Rev.*, 2008, **37**, 320–330; (*f*) I. Ojima, *Fluorine in Medicinal Chemistry and Chemical Biology*, Wiley-Blackwell, Chichester, U.K., 2009; (*g*) D. O'Hagan, *J. Fluorine Chem.*, 2010, **131**, 1071–1081.

2 (*a*) K. L. Kirk, *Org. Process Res. Dev.*, 2008, **12**, 305–321; (*b*) T. Furuya, J. E. M. N. Klein and T. Ritter, *Synthesis*, 2010, 1804–1821.

3 (*a*) V. V. Grushin, *Chem.–Eur. J.*, 2002, **8**, 1006–1014; (*b*) V. V. Grushin, *Acc. Chem. Res.*, 2010, **43**, 160–171.

4 D. A. Watson, M. Su, G. Teverovskiy, Y. Zhang, J. García-Fortanet, T. Kinzel and S. L. Buchwald, *Science*, 2009, **325**, 1661–1664.

5 (*a*) N. D. Ball and M. S. Sanford, *J. Am. Chem. Soc.*, 2009, **131**, 3796–3797; (*b*) T. Furuya, D. Benitez, E. Tkatchouk, A. E. Strom, P. Tang, W. A. Goddard, III and T. Ritter, *J. Am. Chem. Soc.*, 2010, **132**, 3793–3807.

6 We exclude from discussion here the HDF of heteroaromatic substrates such as pentafluoropyridine for which there is a rich reaction chemistry. See ref. 7*b–e* and references therein.

7 (*a*) W. D. Jones, *Dalton Trans.*, 2003, 3991–3995; (*b*) R. N. Perutz and T. Braun, in *Comprehensive Organometallic Chemistry III*, ed. R. H. Crabtree and D. M. P. Mingos, Elsevier, Oxford, 2007, pp. 725–758; (*c*) E. Clot, O. Eisenstein, N. Jasim, S. A. Macgregor, J. E. McGrady and R. N. Perutz, *Acc. Chem. Res.*, 2011, **44**, 333–348; (*d*) A. Nova, R. Mas-Ballesté and A. Lledós, *Organometallics*, 2012, **31**,

1245–1256; (*e*) D. Lentz, T. Braun and M. F. Kuehnel, *Angew. Chem. Int. Ed.*, 2013, DOI: 10.1002/anie.201205260.
8 B. L. Edelbach, A. K. F. Rahman, R. J. Lachicotte and W. D. Jones, *Organometallics*, 1999, **18**, 3170–3177.
9 (*a*) B. M. Kraft, R. J. Lachicotte and W. D. Jones, *J. Am. Chem. Soc.*, 2001, **123**, 10973–10979; (*b*) B. M. Kraft and W. D. Jones, *J. Organomet. Chem.*, 2002, **658**, 132–140.
10 (*a*) J. L. Kiplinger and T. G. Richmond, *Chem. Commun.*, 1996, 1115–1116; (*b*) J. L. Kiplinger and T. G. Richmond, *J. Am. Chem. Soc.*, 1996, **118**, 1805–1806.
11 M. K. Whittlesey, R. N. Perutz, B. Greener and M. H. Moore, *Chem. Commun.*, 1997, 187–188.
12 S. Hintermann, P. S. Pregosin, H. Rüegger and H. C. Clark, *J. Organomet. Chem.*, 1992, **435**, 225–234.
13 B. L. Edelbach and W. D. Jones, *J. Am. Chem. Soc.*, 1997, **119**, 7734–7742.
14 L. Maron, E. L. Werkema, L. Perrin, O. Eisenstein and R. A. Andersen, *J. Am. Chem. Soc.*, 2005, **127**, 279–292.
15 M. Aizenberg and D. Milstein, *Science*, 1994, **265**, 359–361.
16 M. Aizenberg and D. Milstein, *J. Am. Chem. Soc.*, 1995, **117**, 8674–8675.
17 J. Vela, J. M. Smith, Y. Yu, N. A. Ketterer, C. J. Flaschenriem, R. J. Lachicotte and P. L. Holland, *J. Am. Chem. Soc.*, 2005, **127**, 7857–7870.
18 (*a*) S. A. Johnson, C. W. Huff, F. Mustafa and M. Saliba, *J. Am. Chem. Soc.*, 2008, **130**, 17278–17279; (*b*) S. A. Johnson, E. T. Taylor and S. J. Cruise, *Organometallics*, 2009, **28**, 3842–3855.
19 P. Fischer, K. Götz, A. Eichhorn and U. Radius, *Organometallics*, 2012, **31**, 1374–1383.
20 (*a*) H. Lv, J.-H. Zhan, Y.-B. Cai, Y. Yu, B. Wang and J.-L. Zhang, *J. Am. Chem. Soc.*, 2012, **134**, 16216–16227; (*b*) J.-H. Zhan, H. Lv, Y. Yu and J.-L. Zhang, *Adv. Synth. Catal.*, 2012, **354**, 1529–1541.
21 S. Yow, S. J. Gates, A. J. P. White and M. R. Crimmin, *Angew. Chem., Int. Ed.*, 2012, **51**, 12559–12563.
22 NHC abbreviations: SIMes = 1,3-bis-(2,4,6-trimethylphenyl)-imidazolin-2-ylidene; SIPr = 1,3-bis-(2,6-diisopropylphenyl)-imidazolin-2-ylidene; IPr = 1,3-bis-(2,6-diisopropylphenyl)-imidazol-2-ylidene; IMes = 1,3-bis-(2,4,6-trimethylphenyl)-imidazol-2-ylidene; IMe = 1,3-bis-(methyl)imidazol-2-ylidene.
23 S. P. Reade, M. F. Mahon and M. K. Whittlesey, *J. Am. Chem. Soc.*, 2009, **131**, 1847–1861.
24 J. A. Panetier, S. A. Macgregor and M. K. Whittlesey, *Angew. Chem., Int. Ed.*, 2011, **50**, 2783–2786.
25 M. J. Frisch, G. W. Trucks, H. B. Schlegel, G. E. Scuseria, M. A. Robb, J. R. Cheeseman, J. J. A. Montgomery, T. Vreven, K. N. Kudin, J. C. Burant, J. M. Millam, J. T. S. S. Iyengar, V. Barone, B. Mennucci, M. Cossi, G. Scalmani, N. Rega, G. A. Petersson, H. Nakatsuji, M. Hada, M. Ehara, K. Toyota, R. Fukuda, J. Hasegawa, M. Ishida, T. Nakajima, Y. Honda, O. Kitao, H. Nakai, M. Klene, X. Li, J. E. Knox, H. P. Hratchian, J. B. Cross, V. Bakken, C. Adamo, J. Jaramillo, R. Gomperts, R. E. Stratmann, O. Yazyev, A. J. Austin, R. Cammi, C. Pomelli, J. W. Ochterski, P. Y. Ayala, K. Morokuma, G. A. Voth, P. Salvador, J. J. Dannenberg, V. G. Zakrzewski, S. Dapprich, A. D. Daniels, M. C. Strain, O. Farkas, D. K. Malick, A. D. Rabuck, K. Raghavachari, J. B. Foresman, J. V. Ortiz, Q. Cui, A. G. Baboul, S. Clifford, J. Cioslowski, B. B. Stefanov, G. Liu, A. Liashenko, P. Piskorz, I. Komaromi, R. L. Martin, D. J. Fox, T. Keith, M. A. Al-Laham, C. Y. Peng, A. Nanayakkara, M. Challacombe, P. M. W. Gill, B. Johnson, W. Chen, M. W. Wong, C. Gonzalez and J. A. Pople, *GAUSSIAN 03 (Revision C.02)*, Gaussian, Inc., Wallingford, CT, 2004.
26 (*a*) J. P. Perdew, *Phys. Rev. B: Condens. Matter*, 1986, **33**, 8822–8824; (*b*) A. D. Becke, *Phys. Rev. A*, 1988, **38**, 3098–3100.
27 D. Andrae, U. Häußermann, M. Dolg, H. Stoll and H. Preuß, *Theor. Chim. Acta*, 1990, **77**, 123–141.
28 A. Höllwarth, M. Böhme, S. Dapprich, A. W. Ehlers, A. Gobbi, V. Jonas, K. F. Köhler, R. Stegmann, A. Veldkamp and G. Frenking, *Chem. Phys. Lett.*, 1993, **208**, 237–240.
29 (*a*) W. J. Hehre, R. Ditchfield and J. A. Pople, *J. Chem. Phys.*, 1972, **56**, 2257–2261; (*b*) P. C. Hariharan and J. A. Pople, *Theor. Chim. Acta*, 1973, **28**, 213–222.
30 J. Tomasi, B. Mennucci and R. Cammi, *Chem. Rev.*, 2005, **105**, 2999–3093.
31 Computed free energies confirm the preference for reaction via the stepwise pathway, the barrier being 65.0 kJ mol^{-1} compared to 85.0 kJ mol^{-1} for the concerted pathway.
32 The corresponding solvent-corrected free energy activation barriers are 65.0 kcal mol^{-1}, 74.5 kJ mol^{-1} and 70.3 kJ mol^{-1} for reaction at the *ortho*-, *meta*- and *para*-positions respectively.
33 (*a*) E. Clot, M. Besora, F. Maseras, C. Mégret, O. Eisenstein, B. Oelckers and R. N. Perutz, *Chem. Commun.*, 2003, 490–491; (*b*) E. Clot, C. Mégret, O. Eisenstein and R. N. Perutz, *J. Am. Chem. Soc.*, 2009, **131**, 7817–7827.
34 In computing the bond dissociation energies the geometries of the $C_6F_{5-n}H_n$ radicals were fully optimised.
35 This trend is consistent with the available experimental data (C_6F_6: BDE = 485 ± 25 kJ mol^{-1}; C_6H_5F: BDE = 525.5 ± 8.4 kJ mol^{-1}). See: *Handbook of Bond Dissociation Energies in Organic Compounds*, ed. Y.-R. Luo, CRC Press, 2003.
36 In all cases, when there is a choice, we have only considered the orientation of the fluoroarene that directs the *ortho*- or *meta*-C–H bonds towards the NHC ligand.
37 Although the computed barriers are always higher along the concerted pathway, it is noticeable that a preference for reaction at sites with two *ortho*-F substituents is retained for this mechanism, as seen with Model 3.